Electrochimica Acta 63 (2012) 55–63

Contents lists available at SciVerse ScienceDirect

Electrochimica Acta

journal homepage: www.elsevier.com/locate/electacta

Intrinsic limitations of impedance measurements in determining electric double layer capacitances

Hainan Wang, Laurent Pilon*

University of California, Henry Samueli School of Engineering and Applied Science, Mechanical and Aerospace Engineering Department, 420 Westwood Plaza, Los Angeles, CA 90095, USA

ARTICLE INFO

Article history:
Received 23 August 2011
Received in revised form
11 December 2011
Accepted 12 December 2011
Available online 20 December 2011

Keywords:
Electrochemical impedance spectroscopy
Electric double layer
Electrochemical capacitor
Electric double layer capacitor
RC circuit

ABSTRACT

This paper aims to clarify the intrinsic limitations of electrochemical impedance spectroscopy (EIS) in measuring electric double layer (EDL) capacitance. For more than two decades, capacitances measured using EIS at low frequencies have been reported to be significantly smaller than those measured using other techniques without any definitive explanations. In this paper, EIS measurements were numerically reproduced for electric double layers formed near a planar electrode in aqueous electrolyte solutions. The transient double layer dynamics was simulated for low and large electrolyte concentrations using the classical Poisson–Nernst–Planck (PNP) model with or without a Stern layer, and a modified PNP model with a Stern layer, respectively. A characteristic time for ion diffusion τ_m was identified as λ_m^2/D where λ_m is the Debye length based on the maximum ion concentration. For a given concentration, the predicted capacitance and the phase shift of surface charge density plotted versus dimensionless frequency $\tau_m f$ for various values of diffusion coefficient overlapped on a single line. This was true for all models considered with or without Stern layer. The simulated EIS measurements systematically overestimated the EDL capacitance for dilute electrolyte solutions while they underestimated it for concentrated electrolyte solutions subject to large electric potential. This discrepancy can be attributed to the fact that the RC circuit used in EIS to model electric double layers is not valid. This study established that the EIS measurements have intrinsic limitations and are inadequate for accurately determining EDL capacitances for practical applications with large potentials such as electrochemical capacitors.

1. Introduction

Electrochemical impedance spectroscopy (EIS) is a powerful tool in the field of electrochemistry [1–5]. It has been used extensively to characterize the performance of various electrical energy storage devices such as electrochemical capacitors (also known as supercapacitors) [6–14], batteries [15–17], and fuel cells [4,18]. In these applications, the charged electrodes are typically immersed in the electrolyte solution. Electric double layers form at the electrode/electrolyte interfaces which are accessible to ions present in the electrolyte. Fig. 1 shows a schematic of the electric double layer structure forming near the surface of an anode. Solvated cations of diameter a migrate and adsorb to the electrode surface due to electrostatic forces [1,19–21]. The Stern layer is defined as the compact layer of immobile ions strongly adsorbed to the electrode surface [1,19–21]. Note that there are no free charges within the Stern layer [1,19,20]. Beyond the Stern layer is the so-called diffuse layer where ions are mobile under the coupled influence of electrostatic forces and diffusion [1,19–21]. Fig. 1b shows the typical representation of an electric double layer capacitance with the Stern layer and diffuse layer capacitances in series [1,6,19,21].

EIS measurements consist of imposing a time harmonic electric potential with a certain frequency at the electrodes. This harmonic potential consists of two components: (i) a time-independent "DC potential" and (ii) a periodically oscillating potential with a small amplitude typically less than 10 mV [4,12,13]. The resulting electric current is recorded. Then, the magnitude of the electrochemical impedance can be defined as the ratio of the amplitudes of oscillating potential and current while its phase angle is the shift by which the current is ahead of the potential [1–4]. A simple RC circuit consisting of a resistor and a capacitor in series is most commonly used to model pure electric double layers (i.e., without Faradic reaction) forming at an electrode as shown in Fig. 1c [1–11]. The resistance and capacitance for a given frequency are retrieved from the in-phase and out-of-phase components of the measured electrochemical impedance, respectively [1–11]. The double layer capacitance measured by EIS is typically plotted as a function of frequency [3,7–12,14,22–31]. It is known to decrease with increasing frequency beyond a critical frequency due to the fact that the double layer is not ideally capacitive at large frequencies [28–31].

* Corresponding author. Tel.: +1 310 206 5598; fax: +1 310 206 2302
E-mail address: pilon@seas.ucla.edu (L. Pilon).

0013-4686/$ – see front matter © 2012 Elsevier Ltd. All rights reserved.
doi:10.1016/j.electacta.2011.12.051

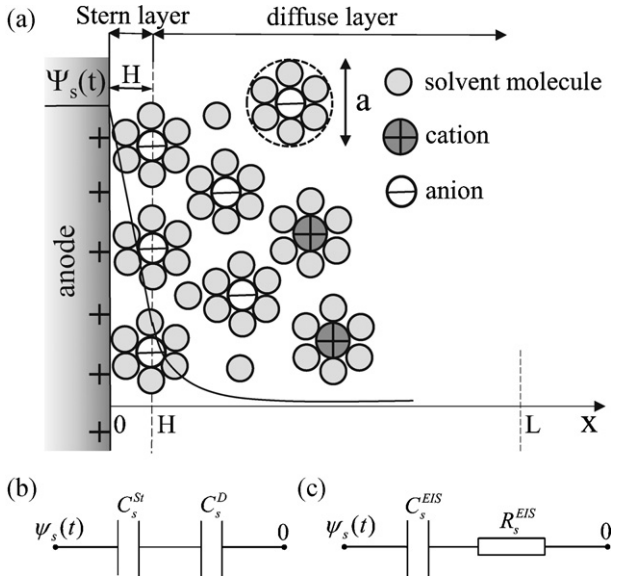

Fig. 1. Schematic of (a) the electric double layer structure showing the arrangement of solvated anions and cations near an anode/electrolyte interface and the simulated computational domain consisting of the Stern layer and the diffuse layer, (b) the Stern and diffuse layer capacitances in series [1,6,19], and (c) the equivalent RC circuit used in EIS [1–4,8].

It has also been referred to as double layer impedance [29–32]. The capacitance retrieved from EIS measurements at low frequencies has been regarded as an estimate of the capacitance at the imposed DC potential [8,9,12,33].

However, capacitances measured using EIS at low frequencies have been reported to systematically underpredict capacitances measured using cyclic voltammetry at low scan rates [22–25,33–35] and galvanostatic charge/discharge at low current density [24–27,36]. This was originally observed in the measurements of pseudocapacitances of different conducting polymers [22,33–36]. It has also been reported for various electrochemical capacitors [23–27,36]. For example, Ren and Pickup [35] summarized the literature measuring the pseudocapacitance of various conducting polymers. They concluded that "*it has been generally observed that the low frequency limiting capacitances observed in AC experiments on conducting polymers are significantly less than those measured by cyclic voltammetry*" [35]. Lufrano et al. [26] measured the capacitance of electric double layer capacitors (EDLCs) with electrodes made of carbon composite. Three electrolytes were used including commercial Nafion 115, recast Nafion membrane, and H_2SO_4 aqueous solution. The authors observed that the EDLC capacitances measured using EIS were smaller than those measured using galvanostatic charge/discharge and "*the maximum difference of the capacitance is in the order of* 20% *for all capacitors*" [26].

The origin of this discrepancy has been "*a subject of some controversy for more than two decades*" [36]. Various hypotheses have been proposed attempting to explain these observations [22,34–40] including (i) the presence of "deeply trapped" counterions remaining immobile in EIS experiments [22,38], (ii) "conformation changes" of electrode materials [35,39], and (iii) large hindrance to AC current penetration into porous electrodes [25,27], to name a few. However, there is still no clear and definitive explanations to the observed discrepancies. Accordingly, EIS has been regarded as "*the least reliable and accurate technique for determining the supercapacitive properties of materials*" [36]. In addition, to the best of our knowledge, no studies have attempted to elucidate this question via physics-based numerical simulations.

This paper aims to clarify the intrinsic limitations of EIS for determining the electric double layer capacitances. The EIS measurements were simulated by modeling ion transport in electrolyte solutions as a function of frequency. The results were compared with analytical expressions for capacitances under equilibrium conditions.

2. Background

2.1. Electrochemical impedance spectroscopy

In EIS measurements, the electric potential $\psi_s(t)$ imposed at the electrode is a harmonic function of time t. This results in a harmonic current density J_s (in A/m^2) provided that the amplitude of the harmonic potential is small enough (e.g., less than 10 mV). Using complex notations, the imposed electric potential and the corresponding current density can be expressed as [1–4],

$$\psi_s(t) = \psi_{dc} + \psi_0 e^{i2\pi ft} \quad \text{and} \quad J_s(t) = J_{dc} + J_0 e^{i(2\pi ft-\phi)} \tag{1}$$

where ψ_{dc} and J_{dc} are time-independent DC potential and DC current density, respectively. Here, ψ_0 and J_0 are the amplitudes of the potential and current density around their DC components, respectively. The imaginary unit is denoted by i, f is the frequency expressed in Hz, while $\phi(f)$ is the frequency-dependent phase angle between the harmonic potential $\psi_s(t)$ and the current density $J_s(t)$. The complex electrochemical impedance Z is defined as [1–4],

$$Z = \frac{\psi_0}{J_0} e^{i\phi} = Z' + iZ'' \tag{2}$$

where Z' and Z'' (expressed in Ω m^2) are the real and imaginary parts of the impedance, respectively. Based on the equivalent RC circuit shown in Fig. 1c, the resistance and capacitance per unit surface area (also called specific resistance and capacitance) are given by [1–4,8],

$$R_s^{EIS} = Z' \quad \text{and} \quad C_s^{EIS} = \frac{-1}{2\pi f Z''} \tag{3}$$

Eq. (3) is the most commonly used formula to determine the capacitance of EDLCs from EIS measurements [7–11,36]. Alternatively, more complicated RC circuits [6,41,42] or transmission line models [6,43–48] have also been developed to represent electric double layers by introducing more resistor and capacitor components. Then, these models have to be fitted with experimental EIS data to retrieve the resistances and capacitances. However, these models suffer from other drawbacks as stated in Ref. [49]: *"First, it is possible for two different models to produce the same impedance response [...]. Second, the overall impedance expressions corresponding to most models give little or no direct information about the physical meaning of the elements for such models."* Note also that the fitted pseudocapacitance values based on complex RC circuits were also reported to underpredict those measured using other techniques [37–40,50].

2.2. Ion transport in electrolyte solutions

It is well known that ion transport in dilute electrolyte solutions can be accurately described by the classical Poisson–Nernst–Planck (PNP) model [1,51–53]. The PNP model has been used extensively to investigate EIS and reaction kinetics of one-dimensional electrolytic cells [29–32,54] and ion-exchange membranes [55–59]. However, the PNP model neglects the finite size of ions and treat ions as point-charges. This assumption is appropriate only when both the ion concentration c_∞ and the electric potential are small [52,53].

Recently, efforts have been made to account for the effect of finite ion size in modeling ion transport in concentrated electrolyte solutions. Lim et al. [60,61] used the classical Nernst–Planck model and accounted for the finite ion size by adding a Stern layer. Their

model imposed linear potential profile and uniform ion concentrations in the Stern layer. However, it was limited to relatively low surface potential and electrolyte concentration, i.e., $\psi_s \leq 0.2$ V and $c_\infty \leq 0.01$ mol/L. Kilic et al. [52] derived a modified PNP (MPNP) model valid for binary and symmetric electrolytes under large electrolyte concentration and electric potential. They added an excess term in the expression of the electrochemical potential to account for the finite ion size. They solved the MPNP model numerically for a planar electrode and predicted the profiles of electric potential and ion concentrations in the diffuse layer [52]. Their results demonstrated that under large electrolyte concentration and electric potential, the predictions of PNP model deviated significantly from the MPNP model due to the point-charge assumption. Alternatively, Horno and co-workers [62,63] accounted for the finite ion size in ion mass fluxes using the activity coefficient. It was later demonstrated that Kilic's model [52] can be formulated in a form equivalent to that based on activity coefficient [53,64]. However, to the best of our knowledge, no studies have simulated EIS measurements under both large electrolyte concentrations and electric potential other than by using RC circuits [6,8,9] or transmission line models [6,45–48].

This paper aims (i) to simulate the electric double layer dynamics in EIS measurements and (ii) to understand the limitations of EIS in determining electric double layer capacitances. The transient double layer dynamics was simulated for the electric double layer formed near a planar electrode in aqueous electrolyte solutions. For low electrolyte concentrations, the classical Poisson–Nernst–Planck (PNP) model with or without a Stern layer was solved. Instead, for large electrolyte concentrations, a modified PNP model [52] was used accounting for a Stern layer.

3. Analysis

3.1. Schematics and assumptions

Fig. 1a shows the schematic of the computational domain simulating a planar electrode immersed in an electrolyte solution. The region of electrolyte solution consists of two layers corresponding to (1) a Stern layer of thickness H near the electrode surface and (2) a diffuse layer beyond. A time-dependent electric potential $\psi_s(t)$ was prescribed at the electrode surface and was zero far away from the electrode surface. The length of the overall computational domain was specified to be (i) $L = 160$ nm for electrolyte concentration c_∞ less than 0.01 mol/L and (ii) $L = 80$ nm for $c_\infty = 1$ mol/L. Note that the electric double layer thickness decreases with increasing electrolyte concentration [20,52,53]. Increasing the value of L by a factor of two was found to have no effect on the predicted specific capacitance C_s under equilibrium conditions and capacitance C_s^{EIS} retrieved from EIS simulations at low frequency using Eq. (3). However, the values of C_s^{EIS} predicted at large frequencies were found to decrease with increasing L. This can be attributed to the fact that the charge storage or charge relaxation took longer as the domain length L increased under large frequencies [65]. Then, the charge storage at large frequencies was limited as it could not follow the fast variation in the electric potential.

To make the problem mathematically tractable, the following assumptions were made: (1) anions and cations had the same effective diameter and diffusion coefficient which were assumed to be constant and independent of electrolyte concentration [53,66,67], (2) the electrolyte relative permittivity was constant, independent of frequency, and equals to that of water. Note that the relative permittivity of water at room temperature is known to significantly decrease for frequency larger than 5×10^9 Hz [68]. The frequency range considered here did not exceed this value except otherwise mentioned, (3) isothermal conditions prevailed throughout the electrode and electrolyte, (4) advection of the electrolyte was assumed to be negligible, (5) the ions could only accumulate at the electrode surface and could not diffuse into the electrode, i.e., there was no ion insertion, and (6) the specific ion adsorption due to non-electrostatic forces were assumed to be negligible.

3.2. Governing equation and boundary conditions

The local electric potential $\psi(x, t)$ and ion concentrations $c_i(x, t)$ in the electrolyte solution were computed by solving (i) the Poisson equation in the Stern and diffuse layers [19,60,61] and (ii) the PNP or MPNP model in the diffuse layer for small or large electrolyte concentration, respectively [52,53,64]. For binary and symmetric electrolytes, the valency is such that $z_1 = -z_2 = z$ and the bulk ion concentration is given by $c_{1\infty} = c_{2\infty} = c_\infty$. Then, assuming identical diffusion coefficient $D_1 = D_2 = D$, the MPNP model with Stern layer can be written as [52,53,64],

$$\frac{\partial}{\partial x}\left(\epsilon_0\epsilon_r \frac{\partial \psi}{\partial x}\right) = \begin{cases} 0 & \text{for} \quad 0 \leq x < H \quad (4a) \\ eN_A z(c_1 - c_2) & \text{for} \quad x \geq H \quad (4b) \end{cases}$$

$$\frac{\partial c_i}{\partial t} = \frac{\partial}{\partial x}\left(D\frac{\partial c_i}{\partial x} + \frac{z_i D}{R_u T} F c_i \frac{\partial \psi}{\partial x} + \frac{\nu D c_i}{2c_\infty - \nu(c_1 + c_2)} \frac{\partial (c_1 + c_2)}{\partial x}\right) \quad \text{for} \quad x \geq H \quad (4c)$$

where $c_i(x, t)$ is the local molar concentration of ion species "i" ($i = 1, 2$). The Cartesian coordinate is denoted by x while ϵ_0 and ϵ_r are the free space permittivity ($\epsilon_0 = 8.854 \times 10^{-12}$ F/m) and the relative permittivity of the electrolyte solution, respectively. The absolute temperature is denoted by T, e is the elementary charge ($e = 1.602 \times 10^{-19}$ C), N_A is the Avogadro's number ($N_A = 6.022 \times 10^{23}$ mol^{-1}) while F and R_u are the Faraday constant ($F = eN_A$ sA/mol) and the universal gas constant ($R_u = 8.314$ J K^{-1} mol^{-1}), respectively. The packing parameter is defined as $\nu = 2a^3 N_A c_\infty$ where a is the effective ion diameter. It represents the ratio of the total bulk ion concentration to the maximum ion concentration $c_m = 1/N_A a^3$ assuming a simple cubic ion packing [52,53,64]. Therefore, ν should not be larger than unity for the model to be physically acceptable [52,53,64]. Eqs. (4b) and (4c) reduce to the classical Poisson–Nernst–Planck model when $\nu = 0$ [52,53,64]. Note that in Refs. [52,53,64], the Stern layer was accounted for via a boundary condition relating the potential drop across the Stern layer and the potential gradient at the Stern/diffuse layer interface. Here, the electric potential in the Stern layer was solved explicitly. In fact, these two approaches are equivalent for planar electrodes [52,53,64].

Moreover, the associated boundary and initial conditions were given by [19,51,52],

$$\psi(x = 0, t) = \psi_s(t), \quad (5a)$$

$$\psi|_{x=H^-} = \psi|_{x=H^+} \quad \text{and} \quad \epsilon_0\epsilon_r \frac{d\psi}{dx}|_{x=H^-} = \epsilon_0\epsilon_r \frac{d\psi}{dx}|_{x=H^+}, \quad (5b)$$

$$D\frac{\partial c_i}{\partial x} + \frac{z_i D}{R_u T} F c_i \frac{\partial \psi}{\partial x} + \frac{\nu D c_i}{2c_\infty - \nu(c_1 + c_2)} \frac{\partial (c_1 + c_2)}{\partial x} = 0, \text{ at } x = H \quad (5c)$$

$$\psi(x = L, t) = 0 \quad \text{and} \quad c_i(x = L, t) = c_\infty, \quad (5d)$$

$$\psi(x, t = 0) = 0 \quad \text{and} \quad c_i(x, t = 0) = c_\infty, \quad \text{for} \quad 0 \leq x \leq L \quad (5e)$$

Note that the surface electric potential $\psi_s(t)$ in Eq. (5a) was given by Eq. (1). Eq. (5b) states that the electric potential and displacement were continuous across the Stern/diffuse layer interface located at $x = H$ [19,51]. Eq. (5c) indicates that the mass fluxes vanish for both ion species at the electrode surface since there is no ion insertion [assumption (6)] [52,53]. Note that, when $H = 0$ nm, Eqs. (4) and (5) correspond to simulations without the Stern layer.

3.3. Constitutive relations

In order to solve Eqs. (4) and (5), the electrolyte properties ϵ_r, z, c_∞, a and D along with the temperature T and the surface potential $\psi_s(t)$ are needed. The present study focuses on aqueous electrolyte solution at room temperature (T = 298 K) with ϵ_r = 78.5 [68]. Note that the electrolyte dielectric permittivity decreases at large local electric field [69,70]. The electric double layer capacitance may decrease by a factor two or three when accounting for this effect [69,70]. However, this is not expected to affect either the comparison between the capacitance under equilibrium conditions and that retrieved from EIS simulations or the qualitative conclusions of the present study.

The effective ion diameter and diffusion coefficient were taken as a = 0.66 nm [67] and $D = 2\times10^{-9}$ m^2/s [68], respectively, while the valency was z = 1. These values correspond to solvated ions such as K^+ and Cl^- in aqueous solutions. The diffusion coefficients of ions such as K^+ and Cl^- are known to decrease by about 10% when increasing the electrolyte concentration from 0 to 1 mol/L [71]. In addition, ion diffusion coefficients significantly decrease in the presence of charged obstacles [72] or porous electrodes [73]. Here, a parametric study was also carried out for other values of diffusion coefficient, namely, $D = 2\times10^{-8}$ and 2×10^{-10} m^2/s. The electrolyte concentration was chosen as (i) c_∞ = 0.01 and 0.001 mol/L so that the classical PNP model was valid and (ii) c_∞ = 1.0 mol/L corresponding to typical values in actual electrochemical capacitors. In addition, the Stern layer thickness H was approximated as the radius of solvated ions [1,20,21], i.e., $H = a/2$ = 0.33 nm.

Moreover, the DC potential component ψ_{dc} of the harmonic surface electric potential $\psi_s(t)$ was varied from 0.01 to 0.5 V. A DC potential of ψ_{dc} = 0.5 V corresponds to a typical potential difference of 1 V between the anode and the cathode for aqueous electrochemical capacitors. The amplitude of the potential oscillation was taken as (i) ψ_0 = 0.001 V for $\psi_{dc} \le 0.1$ V and (ii) ψ_0 = 0.005 V for $\psi_{dc} > 0.1$ V. Decreasing ψ_0 by up to a factor five was found to have no effect on the predicted impedance and capacitance.

Finally, note that for low electrolyte concentrations c_∞ = 0.001–0.01 mol/L, the frequency range explored in the present study was f = 10–10^7 Hz. It was similar to the range f = 1–10^7 Hz in the experiments used for planar electrodes of gold platted stainless steel in 0.001–0.01 mol/L KCl and $BaCl_2$ electrolyte solutions [74]. For c_∞ = 1 mol/L, frequency ranged from 10^3 to 10^9 Hz due to the significant decrease in the electrical resistance to ion transport when increasing electrolyte concentration [55,75] as discussed in Section 4.2. However, these frequency ranges were several orders of magnitude larger than those encountered in typical EIS measurements for electrochemical capacitors with mesoporous electrodes where the frequency typically ranges from 10^{-3} to 10^5 Hz [9–13,25]. The difference is due to the fact that the electrode was not simulated in the present study. The electrical resistance of the mesoporous electrodes is significantly larger than that of planar electrodes. This, in turn, limits the range of frequencies in EIS measurements of practical EDLCs [8–11].

3.4. Method of solution and data processing

Eq. (4) were solved using the commercial finite element solver COMSOL 3.5a, along with the boundary and initial conditions given by Eq. (5). The capacitance under equilibrium conditions and the capacitance determined using EIS simulations were computed as follows.

3.4.1. Capacitance under equilibrium conditions

The double layer capacitance under equilibrium conditions corresponds to the time-independent surface potential, i.e., $\psi_s(t) = \psi_{dc}$. Then, the Stern and diffuse layer specific capacitances C_s^{St} and C_s^D are defined by dividing the surface charge density [1,20,51,76,77] $q_s(x) = \epsilon_0\epsilon_r E(x)$ by their respective potential difference [1,51,69]. Here, $E(x) = |-d\psi/dx|$ is the norm of the local electric field. The capacitances C_s^{St} and C_s^D of planar electrodes assuming constant electrolyte properties and accounting for the finite ion size are given by [1,51,53,66,69],

$$C_s^{St} = \frac{q_s(0)}{\psi_s - \psi_D} = \frac{\epsilon_0\epsilon_r}{H} \tag{6a}$$

$$C_s^D = \frac{q_s(H)}{\psi_D} = \frac{2zeN_Ac_\infty\lambda_D}{\psi_D}\sqrt{\frac{2}{\nu}\log\left[1+2\nu\sinh^2\left(\frac{ze\psi_D}{2k_BT}\right)\right]} \tag{6b}$$

where $\psi_D = \psi(H)$ is the electric potential computed at the Stern layer/diffuse layer interface $x = H$ by solving the steady-state equilibrium modified Poisson–Boltzmann model at surface potential ψ_{dc} and electrolyte concentration c_∞ [52,53,66,69]. Then, the total specific capacitance C_s was calculated using the series formula as [1,51,69],

$$\frac{1}{C_s} = \frac{1}{C_s^{St}} + \frac{1}{C_s^D} \tag{7}$$

Note that $\psi_D = \psi_{dc}$ when computing the capacitance C_s^D (Eq. (6b)) without the Stern layer. Note also that the so-called differential capacitance defined as $C_d = dq_s/d\psi$ is different from the capacitance given by Eqs. (6) and (7) for double layers [1,51,66] and C_s^{EIS} investigated in the present study.

3.4.2. Simulating EIS measurements

EIS measurements were simulated by numerically imposing the harmonic surface electric potential given by Eq. (1). The corresponding transient surface current density was estimated as [32,55,56,76–81],

$$J_s(t) = \frac{dq_s}{dt} = \epsilon_0\epsilon_r\frac{dE_s}{dt} \tag{8}$$

where $E_s(t) = -\left(\partial\psi/\partial x\right)(x=0,t)$ is the electric field at the electrode surface x = 0 at time t. Simulations of EIS measurements were run for at least 50 periods (i.e., $t \ge 50/f$) to ensure the current density and impedance had reached their stationary and periodic states. Then, the electrochemical impedance Z as well as the associated specific capacitance C_s^{EIS} were computed using Eqs. (2) and (3), respectively. The convergence criterion was defined such that the maximum relative difference in the predicted C_s^{EIS} was less than 2% when (1) multiplying the total number of finite elements by two, (2) dividing the time step by two, and (3) running the EIS simulations for 50 more periods. The time step was imposed to be $\Delta t \lesssim 1/400f$. The mesh size was smallest at the electrode surface due to large potential gradient and then gradually increased. The maximum mesh size was specified to be 0.01 nm at the electrode surface and 1 nm in the rest of the domain. The total number of finite elements was less than 300 for all cases simulated in the present study.

3.4.3. Validation

The numerical tool was validated based on three cases reported in the literature. First, the predicted equilibrium electric potential profile in the diffuse layer was validated against the exact solution for planar electrodes [19,20,51] with ϵ_r = 78.5, c_∞ = 0.01 and 0.001 mol/L, ν = 0, and ψ_D = 0.1 V. Second, the computed specific capacitances for the Stern and diffuse layers under equilibrium conditions were validated against Eqs. (6a) and (6b) for (i) ψ_s = 0.1 V, c_∞ = 0.01 mol/L, and a = 0.66 nm as well as (ii) ψ_s = 0.5 V, c_∞ = 1 mol/L, and a = 0.66 nm. Third, the predicted transient ion concentration and electric potential profiles were compared with the numerical solutions for planar electrodes using PNP and MPNP

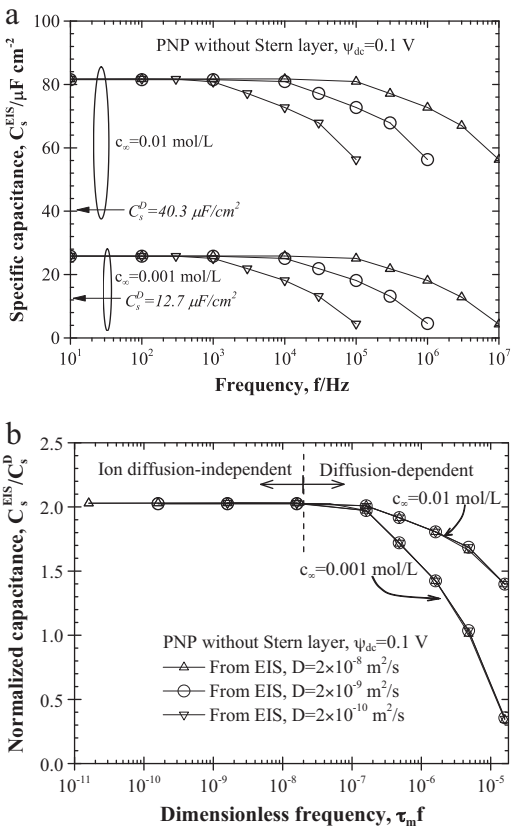

Fig. 2. (a) Specific capacitance determined from EIS simulations as a function of frequency f and (b) normalized specific capacitance C_s^{EIS}/C_s^D as a function of dimensionless frequency $\tau_m f$ for different values of ion diffusion coefficient. Results were obtained by numerically solving the classical PNP model without Stern layer ($H = 0$ nm) for $c_\infty = 0.001$ or 0.01 mol/L and $\psi_{dc} = 0.1$ V. The diffuse layer capacitance C_s^D given by Eq. (6b) is also shown.

models reported in Ref. [52]. Comparison was made for a wide range of packing parameter ν and dimensionless potential ($ze\psi_D/k_BT$). Good agreement was obtained between our results and reported values of $c_i(x, t)$ and $\psi(x, t)$ [52] for all cases considered.

4. Results and discussion

4.1. EIS in dilute electrolyte solutions

4.1.1. Predictions by PNP model without Stern layer

Fig. 2(a) shows the predicted diffuse layer specific capacitance C_s^{EIS} from EIS simulations using Eq. (3) as a function of frequency ranging from 10 to 10^7 Hz. Results were obtained by numerically solving the classical PNP model without the Stern layer, i.e., $\nu = 0$ and $H = 0$ nm. The electrolyte concentration was either $c_\infty = 0.001$ or 0.01 mol/L while $\psi_{dc} = 0.1$ V. The effect of diffusion coefficient was assessed by performing simulations for $D = 2 \times 10^{-8}$, 2×10^{-9}, and 2×10^{-10} m^2/s. Fig. 2(a) demonstrates that, for $D = 2 \times 10^{-8}$ m^2/s, the diffuse layer specific capacitance C_s^{EIS} was independent of frequency for $f \leq 10^5$ Hz for both electrolyte concentrations considered. Then, it decreased with increasing frequency beyond 10^5 Hz. Similarly, for smaller diffusion coefficients $D = 2 \times 10^{-9}$ and 2×10^{-10} m^2/s, C_s^{EIS} was independent of frequency for $f \leq 10^4$ and 10^3 Hz, respectively. Below these frequencies, C_s^{EIS} was independent of diffusion coefficient. This suggests that ion transport by diffusion becomes a limiting factor in charge storage for frequencies larger than a critical frequency which depends on the ion diffusion coefficient D.

Fig. 2(a) also shows the diffuse layer specific capacitance C_s^D under equilibrium conditions given by Eq. (6b) with $\nu = 0$ and equals to 12.7 μF/cm^2 and 40.3 μF/cm^2 for $c_\infty = 0.001$ and 0.01 mol/L, respectively. It is evident that the frequency-independent capacitance C_s^{EIS} overestimated the equilibrium values predicted by Eq. (6b) by more than 100% for both concentrations.

As opposed to a dielectric capacitor, the electric double layer capacitance of porous electrodes is known to depend on frequency. The origin of this so-called "capacitance dispersion" of electrode materials [2,47,48,82–85] has been attributed to various phenomena such as surface inhomogeneity (e.g., defect) [85], surface roughness [2,82–85], pore size distribution in porous electrodes [47,48], as well as specific ion adsorption [2,84], to name a few. However, Fig. 2(a) demonstrates that electric double layers feature capacitance dispersion at high frequencies even for perfectly planar electrodes when only electrostatic phenomena were accounted for. Similar trend was observed in Refs. [28–31] based on the exact solution of the linearized PNP model without Stern layer and assuming zero DC potential. Then, Fig. 2(a) establishes that, besides the above-mentioned mechanisms, the capacitance dispersion can be also attributed to the fact that, at high frequencies, ion transport cannot follow the rapid variations in the electric potential.

Moreover, Fig. 2(b) plots the normalized specific capacitance C_s^{EIS}/C_s^D as a function of dimensionless frequency $\tau_m f$ where τ_m is the characteristic diffusion time scale defined as

$$\tau_m = \frac{\lambda_m^2}{D} \quad \text{with} \quad \lambda_m = \left(\frac{\epsilon_0 \epsilon_r k_B T}{2e^2 z^2 N_A c_m} \right)^{1/2} \tag{9}$$

Here, λ_m is analogous to the Debye length λ_D defined based on the maximum concentration c_m instead of the bulk electrolyte concentration c_∞. The data of C_s^{EIS} and C_s^D were the same as those shown in Fig. 2(a). Note that the traditional diffusion characteristic time is typically defined as $\tau_L = L^2/D$ [65] where the characteristic length is the electrolyte thickness L. Here, τ_L was not the proper characteristic time since the predicted C_s^{EIS} at low frequency was found to be independent of L as previously discussed. In addition, Fig. 2(a) shows that the critical frequency below which C_s^{EIS} is constant was independent of electrolyte concentration c_∞. Then, time scales involving c_∞ are also inadequate including the characteristic time for charge relaxation defined as $\tau_D = \lambda_D^2/D$ [65]. Fig. 2(b) demonstrates that the predicted C_s^{EIS}/C_s^D versus $\tau_m f$ curves for three different diffusion coefficients overlapped for each value of electrolyte concentration considered. Moreover, two regions can be identified in Fig. 2(b). First, for $\tau_m f < 2 \times 10^{-8}$, ion transport is fast enough to follow the variation in the electric potential $\psi_s(t)$ and thus the specific capacitance C_s^{EIS} is independent of frequency. In these cases, C_s^{EIS}/C_s^D was equal to 2.0 regardless of the electrolyte concentration c_∞. Second, for $\tau_m f > 2 \times 10^{-8}$, ion transport was the limiting phenomenon for charge storage and C_s^{EIS} decreased with increasing frequency.

To better understand these results, Fig. 3(a) and (b) shows the imposed surface potential $\psi_s(t)$ and the resulting instantaneous surface charge density $q_s(t) = \epsilon_0 \epsilon_r E_s(t)$ as a function of dimensionless time $t \times f$ ranging from 0 to 10 at two different frequencies, i.e., $f = 10$ and 10^5 Hz. The electrolyte concentration was $c_\infty = 0.01$ mol/L and the diffusion coefficient was taken as $D = 2 \times 10^{-8}$, 2×10^{-9}, or 2×10^{-10} m^2/s. The model and other parameters were identical to those used to generate Fig. 2. Note that the origin of time t was shifted to the time when $q_s(t)$ reached its stationary periodic oscillations. Fig. 3(a) shows that the instantaneous surface charge density $q_s(t)$ was nearly in phase with the imposed surface potential $\psi_s(t)$ at $f = 10$ Hz. At this frequency, the diffusion coefficient had no effect on the predicted $q_s(t)$ and the plots overlap for $D = 2 \times 10^{-8}$ to 2×10^{-10} m^2/s. In addition, Fig. 3(b) shows $q_s(t)$ and $\psi_s(t)$ at high frequency $f = 10^5$ Hz. It is evident that $q_s(t)$ and $\psi_s(t)$ were nearly in

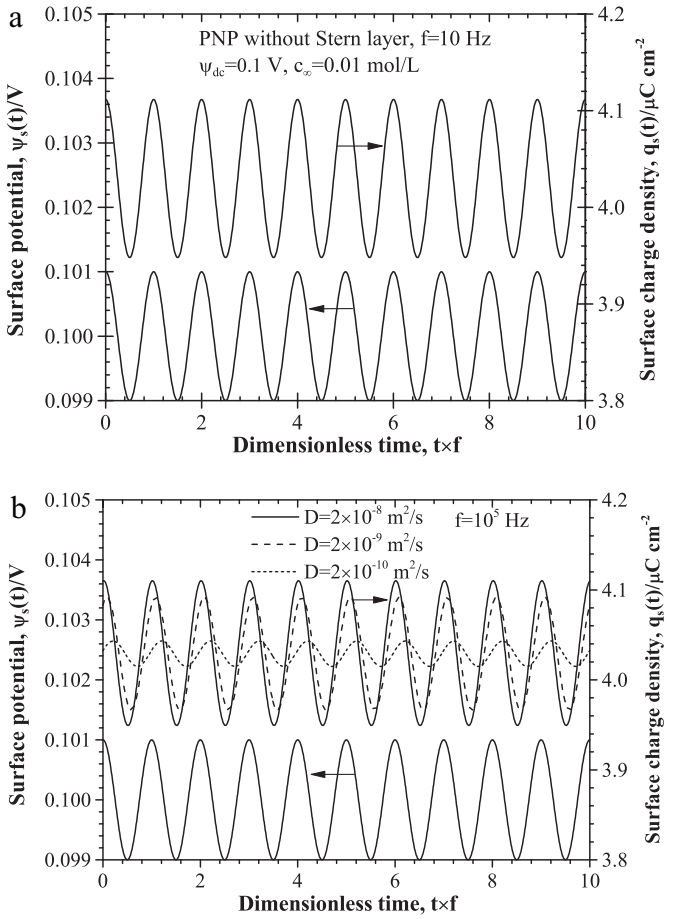

Fig. 3. Imposed surface potential $\psi_s(t)$ and predicted instantaneous surface charge density $q_s(t)$ as a function of dimensionless time $t \times f$ for (a) $f = 10$ Hz and (b) $f = 10^5$ Hz obtained by numerically solving the classical PNP model without Stern layer. The electrolyte concentration was $c_\infty = 0.01$ mol/L while $\psi_{dc} = 0.1$ V and $D = 2 \times 10^{-8}$, 2×10^{-9}, and 2×10^{-10} m^2/s.

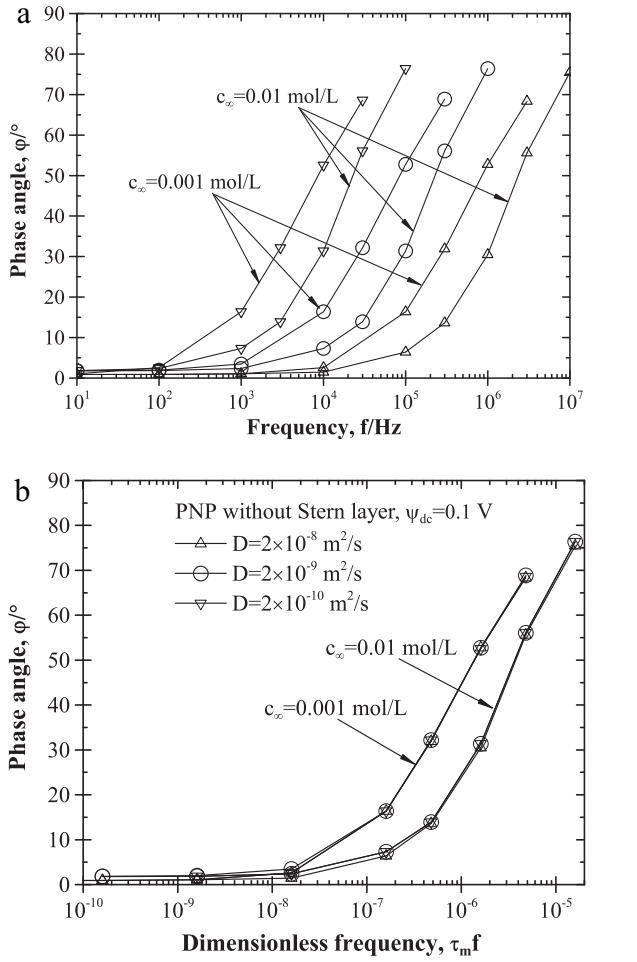

Fig. 4. Predicted phase angle φ between the instantaneous surface charge density $q_s(t)$ and the imposed surface potential $\psi_s(t)$ as a function of (a) frequency f and (b) dimensionless frequency $\tau_m f$. Results were obtained by numerically solving the classical PNP model without Stern layer with $c_\infty = 0.001$ or 0.01 mol/L, $\psi_{dc} = 0.1$ V for $D = 2 \times 10^{-8}$, 2×10^{-9}, and 2×10^{-10} m^2/s.

phase with each other for $D = 2 \times 10^{-8}$ m^2/s. However, they were not in phase for small values of D. The phase depended on the diffusion coefficient. In addition, the amplitude of $q_s(t)$ increased with increasing diffusion coefficient and decreased with increasing frequency. Note that in RC circuits such as those used in EIS, the capacitance was assumed to be either constant or dependent only on frequency [8]. However, the instantaneous diffuse layer specific capacitance computed using $C_s^D(t) = q_s(t)/\psi_s(t)$ also varied harmonically with time (not shown). Consequently, assumptions used for the equivalent RC circuits in EIS are invalid for representing the charging dynamics of electric double layers at high frequencies when $q_s(t)$ and $\psi_s(t)$ are not in phase. This constitutes an inherent limitation of RC circuits and EIS measurements.

Furthermore, Fig. 4(a) shows the predicted phase angle φ between the instantaneous charge density $q_s(t)$ and the imposed surface potential $\psi_s(t)$ for the same frequency range and parameters as those used to generate Fig. 2(a). Fig. 4(a) shows that the phase angle φ was nearly zero at low frequency and increased rapidly beyond a critical frequency. In addition, for a given frequency f, the phase angle decreased with increasing diffusion coefficient D thanks to faster ion transport. It also decreased with increasing electrolyte concentration due to decreasing electrolyte resistance to ionic current [55,75].

Finally, Fig. 4(b) plots the phase angle shown in Fig. 4(a) as a function of the dimensionless frequency $\tau_m f$. Here also, the plots of phase angle φ versus $\tau_m f$ for different values of diffusion coefficient D collapsed on one line for each concentration considered. This confirms that τ_m is the characteristic time for ion diffusion in electric double layer during EIS measurements. Note also that the phase angle of the impedance $\phi(f)$ in Eq. (2) was related to $\varphi(f)$ by $\phi(f) = \varphi(f) - 90^\circ$ (not shown).

4.1.2. Predictions by PNP model with Stern layer

Fig. 5 shows the specific capacitance C_s^{EIS} retrieved from EIS (Eq. (3)) as a function of dimensionless frequency $\tau_m f$ ranging from 10^{-10} to 2×10^{-4} as well as the specific capacitance C_s under equilibrium conditions. Results were obtained by solving the PNP model accounting for a Stern layer of thickness $H = a/2 = 0.33$ nm. The electrolyte concentration was set to be $c_\infty = 0.01$ and 0.001 mol/L, $\psi_{dc} = 0.1$ V while $D = 2 \times 10^{-8}$, 2×10^{-9}, and 2×10^{-10} m^2/s.

The trend of the specific capacitance C_s^{EIS} as a function of $\tau_m f$ was similar to the predictions of PNP model without Stern layer shown in Fig. 2(b). However, the critical dimensionless frequency $\tau_m f$ was larger and equal to 10^{-7} when accounting for the Stern layer. In addition, scaling of C_s^{EIS} by C_s^D, as performed in Fig. 2(b), could not make the ratio C_s^{EIS}/C_s^D collapse on one line for different concentrations. Note also that EIS predictions overestimated the capacitance by 60–80% for different values of c_∞ instead of 100% when the Stern layer was not accounted for (Fig. 2(a)).

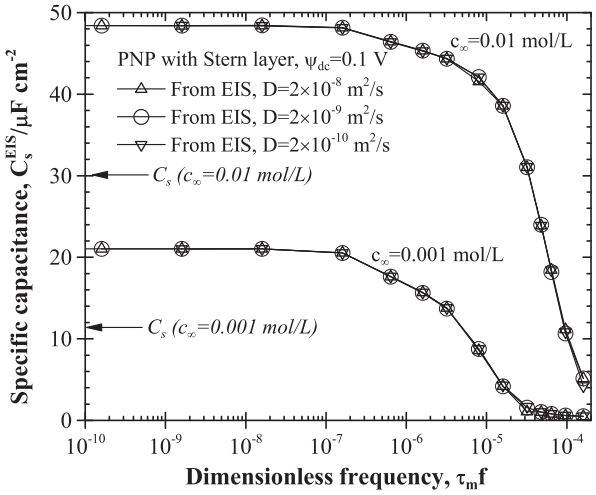

Fig. 5. Predicted specific capacitance C_s^{EIS} determined from EIS (Eq. (3)) as a function of dimensionless frequency $\tau_m f$. Results were obtained by numerically solving the classical PNP model with Stern layer along with the specific capacitance C_s (Eq. (7)) with $c_\infty = 0.01$ and 0.001 mol/L, $H = a/2 = 0.33$ nm, $\psi_{dc} = 0.1$ V, and $D = 2 \times 10^{-8}$, 2×10^{-9}, and 2×10^{-10} m^2/s.

4.2. EIS in concentrated electrolyte solutions

Fig. 6 shows the numerically predicted specific capacitance C_s^{EIS} retrieved from EIS (Eq. (3)) as a function of dimensionless frequency $\tau_m f$ ranging from 10^{-9} to 2×10^{-2}. The results were obtained by solving the MPNP model with a Stern layer (Eqs. (4) and (5)) for $H = a/2 = 0.33$ nm, $c_\infty = 1$ mol/L, $\psi_{dc} = 0.3$ V, and three values of $D = 2 \times 10^{-8}$, 2×10^{-9}, and 2×10^{-10} m^2/s. Fig. 6 also shows the corresponding specific capacitance C_s defined by Eq. (7). Here, the Stern layer and diffuse layer specific capacitances predicted by Eq. (6) were $C_s^{St} = 210.6$ μF/cm^2 and $C_s^{D} = 186.1$ μF/cm^2, respectively, resulting in $C_s = 98.8$ μF/cm^2. Fig. 6 indicates that the specific capacitance C_s^{EIS} for $c_\infty = 1$ mol/L was constant for dimensionless frequency $\tau_m f$ less than 36.4×10^{-4} corresponding to $f = 4 \times 10^7$ Hz. This value should be compared with $\tau_m f = 10^{-7}$ for electrolyte concentrations $c_\infty = 0.01$ and 0.001 mol/L (Fig. 5). The difference can be attributed to the fact that the electrolyte resistance to ionic current decreases significantly as the electrolyte concentration increases and ion transport to and away from the electrode becomes limiting only at very large frequencies. Thus, at high concentrations, ions can respond nearly instantaneously to the rapid variation in electric potential $\psi_s(t)$. Fig. 6 also demonstrates that the specific capacitance decreased sharply for dimensionless frequency $\tau_m f$ larger than 6.4×10^{-4}. It is expected to decrease at much smaller frequencies when simulating the electrode and accounting for its electrical resistance. This was observed in the capacitance versus scan rate curves retrieved in the simulations of cyclic voltammetry in EDLCs [86]. Overall, the characteristic time τ_m given by Eq. (9) is the proper characteristic time scale for low and high concentrations using PNP or MPNP model with or without Stern layer.

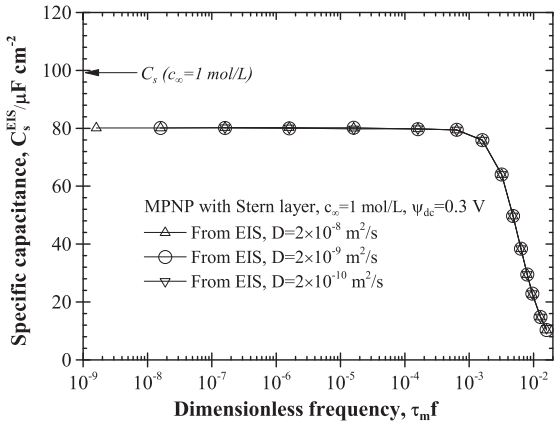

Fig. 6. Predicted specific capacitance C_s^{EIS} determined from EIS (Eq. (3)) as a function of dimensionless frequency $\tau_m f$. Results were obtained by numerically solving the MPNP model with Stern layer along with the specific capacitance C_s (Eq. (7)) with $H = a/2 = 0.33$ nm, $c_\infty = 1$ mol/L, $\psi_{dc} = 0.3$ V, and $D = 2 \times 10^{-8}$, 2×10^{-9}, and 2×10^{-10} m^2/s.

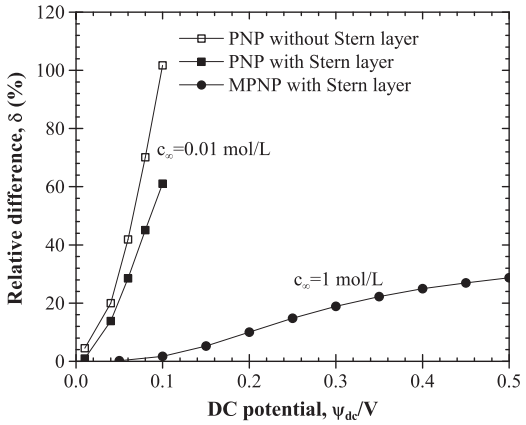

Fig. 7. Relative error between EIS estimates of C_s^{EIS} and double layer capacitance C_s as a function of DC potential obtained by solving (i) the classical PNP model with or without a Stern layer for $c_\infty = 0.01$ mol/L and (ii) the MPNP model with a Stern layer for $c_\infty = 1$ mol/L with $H = a/2 = 0.33$ nm and $D = 2 \times 10^{-9}$ m^2/s.

Moreover, Fig. 6 indicates that EIS measurements underestimated the double layer capacitance by about 20% for $c_\infty = 1$ mol/L and $\psi_{dc} = 0.3$ V. This qualitatively agrees with experimental observations for various electrode materials such as conducting polymers [22,33–40], multi-wall carbon nanotubes and glassy carbons [23], and carbon composites [26] under large electrolyte concentration ($c_\infty \geq 1$ mol/L) and electric potential $\psi_{dc} \sim 0.3 - 1$ V [22–26,33–36].

4.3. Intrinsic limitation of EIS

The previous sections established that EIS measurements overestimated the electric double layer capacitance under low electrolyte concentration (Figs. 2 and 5) while they underestimated it under large electrolyte concentration and electric potential (Fig. 6). This constitutes an intrinsic limitation of EIS measurements for determining the capacitance of EDLCs. It is mainly attributed to the invalidity of the RC circuit and associated assumptions used to predict the electric double layer capacitance.

In order to quantify the intrinsic limitation of EIS in determining double layer capacitance, the relative error was defined as $\delta = \left|(C_s^{EIS} - C_s)/C_s\right|$ where C_s is the total specific capacitance (Eq. (7)) and C_s^{EIS} is that retrieved by EIS using Eq. (3) at low frequency in the diffusion-independent regime.

Fig. 7 shows the computed relative error δ as a function of DC potential ψ_{dc} ranging from 0.01 to 0.5 V. Predictions of C_s^{EIS} for $\psi_{dc} \leq 0.1$ V and $c_\infty = 0.01$ mol/L were obtained by numerically solving the PNP model with or without a Stern layer for frequency $f = 10$ Hz. Predictions of C_s^{EIS} for $\psi_{dc} > 0.1$ V and $c_\infty = 1$ mol/L were obtained by solving the MPNP model with a Stern layer for frequency $f = 10^3$ Hz. It is evident that the relative error increased with increasing DC potential for any model considered. For cases with low DC potential and low concentration based on the PNP model, the relative error was smaller when accounting for the Stern layer. However, it grows rapidly from less than 5% for $\psi_{dc} = 0.01$ V to more than 60% for $\psi_{dc} = 0.1$ V. For concentration $c_\infty = 1$ mol/L and

$\psi_{dc} > 0.1$ V, which are typical of EDLCs, EIS simulations based on the MPNP model with Stern layer underestimated the double layer specific capacitance. In fact, the relative error increased from 0.2% to 45% as the DC potential increased from 0.05 to 0.5 V.

Overall, Fig. 7 indicates that the EIS measurements can predict the double layer capacitance only at very low DC potential and at low frequency. Similar conclusion was drawn by Macdonald [30,31] based on the exact solution of the linearized PNP model without Stern layer and assuming zero DC potential. Note that Macdonald's solution is valid only at very small electrolyte concentration and electric potential due to the point-charge assumption discussed in Section 2.2. This intrinsic limitation can be attributed to the RC circuit used to model electric double layers shown in Fig. 1c. Indeed, previous studies have demonstrated that the RC circuits or transmission line models can accurately represent the linearized PNP model when both the potential and electrolyte concentration are small [29,55,65,75,87–89]. However, these models are not valid under large electric potential. Thus, EIS measurements appears to be inadequate for determining double layer capacitances for practical applications when concentrations and DC potential are typically large such as in electrochemical capacitors for energy storage applications [24,25,27,36].

5. Conclusions

This paper presented numerical simulations of electrochemical impedance spectroscopy measurements for determining the electric double layer capacitance near a planar electrode in aqueous electrolyte solutions. The double layer dynamics was simulated using (i) the PNP model with or without Stern layer for low electrolyte concentrations and electric potential, and (ii) the MPNP model with a Stern layer for large electrolyte concentration and electric potential.

For a given value of electrolyte concentration c_∞, the predicted C_s^{EIS} and impedance phase shift φ plotted versus $\tau_m f$ for various values of ion diffusion coefficient overlapped on a single line for all models considered. Here, the ion diffusion characteristic time was defined as $\tau_m = \lambda_m^2/D$ using the Debye length $\lambda_m = (\epsilon_0 \epsilon_r k_B T/2e^2 z^2 N_A c_m)^{1/2}$ based on the maximum ion concentration c_m. The electric double layer capacitance was found to be constant for dimensionless frequency $\tau_m f$ less than a critical value. However, electric double layers featured an intrinsic "capacitance dispersion" at high frequencies. This was attributed to the fact that ion transport could not follow the fast variation in electric potential.

The EIS simulations overestimated the electric double layer capacitance for dilute electrolyte solutions while they underestimated it for concentrated electrolyte solutions. This corroborates existing experimental observations reporting the discrepancies between EIS measurements [22–27,33–36] and other techniques such as cyclic voltammetry [22–25,33–35] and galvanostatic charge/discharge [25–27,36]. This study established that for large DC potential, the series RC circuit used in EIS to model electric double layer is not valid. Such conditions are typical of energy storage systems such as EDLCs. Then, more reliable techniques such as the galvanostatic charge/discharge and cyclic voltammetry measurements should be preferred in determining the double layer capacitances as recommended in Refs. [24,25,27,36].

Acknowledgement

This material is based upon work supported as part of the Molecularly Engineered Energy Materials, an Energy Frontier Research Center funded by the U.S. Department of Energy, Office of Science, Office of Basic Energy Sciences under Award Number DE-SC0001342.

References

[1] A.J. Bard, L.R. Faulkner, Electrochemical Methods: Fundamentals and Applications, John Wiley & Sons, New York, NY, 2001.
[2] A. Lasia, Electrochemical impedance spectroscopy and its applications, in: B. Conway, J. Bockris, R. White (Eds.), Modern Aspects of Electrochemistry, No. 32, Kluwer Academic Publishers, New York, NY, 2002, p. 143.
[3] M.E. Orazem, B. Tribollet, Electrochemical Impedance Spectroscopy, John Wiley & Sons, Hoboken, New Jersey, 2008.
[4] X.Z. Yuan, C. Song, H. Wang, J. Zhang, Electrochemical Impedance Spectroscopy in PEM Fuel Cells: Fundamentals and Applications, Springer-Verlag, London, UK, 2010.
[5] B.-Y. Chang, S.-M. Park, Annu. Rev. Anal. Chem. 3 (2010) 207.
[6] B.E. Conway, Electrochemical Supercapacitors: Scientific Fundamentals and Technological Applications, Kluwer Academic/Plenum Publishers, New York, NY, 1999.
[7] R. Kotz, M. Carlen, Electrochim. Acta 45 (2000) 2483.
[8] P.L. Taberna, P. Simon, J.F. Fauvarque, J. Electrochem. Soc. 150 (2003) 292.
[9] J. Segalini, B. Daffos, P.L. Taberna, Y. Gogotsi, P. Simon, Electrochim. Acta 55 (2010) 7489.
[10] J.R. Miller, R.A. Outlaw, B.C. Holloway, Science 329 (2010) 1637.
[11] Y. Zhu, S. Murali, M.D. Stoller, K.J. Ganesh, W. Cai, P.J. Ferreira, A. Pirkle, R.M. Wallace, K.A. Cychosz, M. Thommes, D. Su, E.A. Stach, R.S. Ruoff, Science 332 (2011) 1537.
[12] D. Pech, M. Brunet, H. Durou, P. Huang, V. Mochalin, Y. Gogotsi, P.L. Taberna, P. Simon, Nat. Nanotechnol. 5 (2010) 651.
[13] H. Itoi, H. Nishihara, T. Kogure, T. Kyotani, J. Am. Chem. Soc. 133 (2011) 1165.
[14] R.H. Nilson, M.T. Brumbach, B.C. Bunker, J. Electrochem. Soc. 158 (2011) 678.
[15] M.D. Levi, D. Aurbach, J. Phys. Chem. B 101 (1997) 4630.
[16] F.L. Mantia, J. Vetter, P. Novak, Electrochim. Acta 53 (2008) 4109.
[17] J.M. Atebamba, J. Moskon, S. Pejovnik, M. Gaberscek, J. Electrochem. Soc. 157 (2010) 1218.
[18] Z. He, F. Mansfeld, Energy Environ. Sci. 2 (2009) 215.
[19] R.J. Hunter, Foundations of Colloid Science, 2nd ed., Oxford University Press, New York, NY, 2001.
[20] J.H. Masliyah, S. Bhattacharjee, Electrokinetic and Colloid Transport Phenomena, John Wiley & Sons, Hoboken, NJ, 2006.
[21] H.J. Butt, M. Kappl, Surface and Interfacial Forces, Wiley-VCH Verlag GmbH & Co. KGaA, Weinheim, Germany, 2010.
[22] J. Tanguy, J.L. Baudoin, F. Chao, M. Costa, Electrochim. Acta 37 (1992) 1417.
[23] J.P. Zheng, P.C. Goonetilleke, C.M. Pettit, D. Roy, Talanta 81 (2010) 1045.
[24] K. Kierzek, E. Frackowiak, G. Lota, G. Gryglewicz, J. Machnikowski, Electrochim. Acta 49 (2004) 515.
[25] A.B. Fuertes, G. Lota, T.A. Centeno, E. Frackowiak, Electrochim. Acta 50 (2005) 2799.
[26] F. Lufrano, P. Staiti, M. Minutoli, J. Power Sources 124 (2003) 314.
[27] W. Xing, S.Z. Qiao, R.G. Ding, F. Lid, G.Q. Lu, Z.F. Yan, H.M. Cheng, Carbon 44 (2006) 216.
[28] J.D. Ferry, J. Chem. Phys. 16 (1948) 737.
[29] R.P. Buck, J. Electroanal. Chem. 23 (1969) 219.
[30] J.R. Macdonald, Phys. Rev. 92 (1953) 4.
[31] J.R. Macdonald, J. Chem. Phys. 54 (1971) 2026.
[32] I. Rubinstein, B. Zaltzman, Adv. Colloid Interface Sci. 159 (2010) 117.
[33] C. Peng, J. Jin, G.Z. Chen, Electrochim. Acta 53 (2007) 525.
[34] X. Ren, P.G. Pickup, J. Electrochem. Soc. 139 (1992) 2097.
[35] X. Ren, P.G. Pickup, J. Electroanal. Chem. 372 (1994) 289.
[36] A.T. Chidembo, K.I. Ozoemena, B.O. Agboola, V. Gupta, G.G. Wildgoose, R.G. Compton, Energy Environ. Sci. 3 (2010) 228.
[37] I. Rubinstein, E. Sabatani, J. Rishpon, J. Electrochem. Soc. 134 (1987) 3078.
[38] J. Tanguy, N. Mermilliod, M. Hoclet, J. Electrochem. Soc. 134 (1987) 795.
[39] M. Kalaji, L.M. Peter, J. Chem. Soc., Faraday Trans. 87 (1991) 853.
[40] J. Bobacka, A. Lewenstam, A. Ivaska, J. Electroanal. Chem. 489 (2000) 17.
[41] J.R. Macdonald, Electrochim. Acta 35 (1990) 1483.
[42] L.A. Geddes, Ann. Biomed. Eng. 25 (1997) 1.
[43] R. de Levie, Electrochim. Acta 8 (1963) 751.
[44] R. de Levie, in: P. Delahay, C. Tobias (Eds.), Advances in Electrochemical Science and Engineering, vol. 6, Interscience Publishers, New York, NY, 1967, p. 329.
[45] H. Keiser, K.D. Beccu, M.A. Gutjahr, Electrochim. Acta 21 (1976) 539.
[46] I.D. Raistrick, Electrochim. Acta 35 (1990) 1579.
[47] H.K. Song, Y.H. Jung, K.H. Lee, L.H. Dao, Electrochim. Acta 44 (1999) 3513.
[48] H.K. Song, H.Y. Hwang, K.H. Lee, L.H. Dao, Electrochim. Acta 45 (2000) 2241.
[49] J.F. Rubinson, Y.P. Kayinamura, Chem. Soc. Rev. 38 (2009) 3339.
[50] W. Sun, X. Chen, J. Power Sources 193 (2009) 924.
[51] J. Lyklema, Fundamentals of Interface and Colloid Science Solid–Liquid Interfaces, vol. II, Academic Press, San Diego, CA, 2001.
[52] M.S. Kilic, M.Z. Bazant, A. Ajdari, Phys. Rev. E 75 (021503) (2007) 1.
[53] M.Z. Bazant, M.S. Kilic, B.D. Storey, A. Ajdari, Adv. Colloid Interface Sci. 152 (2009) 48.
[54] F.C.M. Freire, G. Barbero, M. Scalerandi, Phys. Rev. E 73 (051202) (2006) 1.
[55] T.R. Brumleve, R.P. Buck, J. Electroanal. Chem. 126 (1981) 73.
[56] R.P. Buck, J. Membr. Sci. 17 (1984) 1.
[57] T. Sokalski, A. Lewenstam, Electrochem. Commun. 3 (2001) 107.
[58] A.A. Moya, Electrochim. Acta 56 (2011) 3015.
[59] V.V. Nikonenko, A.E. Kozmai, Electrochim. Acta 56 (2011) 1262.
[60] J. Lim, J. Whitcomb, J. Boyda, J. Varghese, J. Colloid Interface Sci. 305 (2007) 159.
[61] J. Lim, J. Whitcomb, J. Boyda, J. Varghese, J. Comput. Mech. 43 (2009) 461.

[62] J.J. Lopez-Garcia, M.J. Aranda-Rascon, J. Horno, J. Colloid Interface Sci. 323 (2008) 146.
[63] M.J. Aranda-Rascon, C. Grosse, J.J. Lopez-Garcia, J. Horno, J. Colloid Interface Sci. 336 (2009) 857.
[64] L.H. Olesen, M.Z. Bazant, H. Bruus, Phys. Rev. E 82 (011501) (2010) 1.
[65] M.Z. Bazant, K. Thornton, A. Ajdari, Phys. Rev. E 70 (021506) (2004) 1.
[66] M.S. Kilic, M.Z. Bazant, A. Ajdari, Phys. Rev. E 75 (021502) (2007) 1.
[67] J.N. Israelachvili, Intermolecular and Surface Forces, 3rd ed., Academic Press, San Diego, CA, 2010.
[68] D.R. Lide (Ed.), CRC Handbook of Chemistry and Physics, 90th ed., CRC Press/Taylor & Francis, Boca Raton, FL, 2010.
[69] H. Wang, L. Pilon, J. Phys. Chem. C 115 (2011) 16711.
[70] H. Wang, J. Varghese, L. Pilon, Electrochim. Acta 56 (2011) 6189.
[71] R. Mills, V.M.M. Lobo, Self Diffusion in Electrolyte Solutions: A Critical Examination of Data Compiled from the Literature, Elsevier, New York, NY, 1989.
[72] M. Jardat, B. Hribar-Lee, V. Vlachy, Phys. Chem. Chem. Phys. 10 (2008) 449.
[73] M.C.F. Wander, K.L. Shuford, J. Phys. Chem. C 114 (2010) 20539.
[74] R. Sardenberg, J.M.A. Figueiredo, Electrochim. Acta 55 (2010) 4722.
[75] R.P. Buck, J. Electroanal. Chem. 210 (1986) 1.
[76] D.J. Griffiths, Introduct. Electrodyn., 3rd edition, Prentice Hall, Upper Saddle River, NJ, 1999.
[77] R.P. Feynman, R.B. Leighton, M. Sands, The Feynman Lectures on Physics, vol. 2, 2nd ed., Addison Wesley, New York, NY, 2005.
[78] H. Cohen, J.W. Cooley, Biophys. J. 5 (1965) 145.
[79] T.R. Brumleve, R.P. Buck, J. Electroanal. Chem. 90 (1978) 1.
[80] J.R. Macdonald, J. Chem. Phys. 58 (1973) 4982.
[81] F. Beunis, F. Strubbe, M. Marescaux, J. Beeckman, K. Neyts, A.R.M. Verschueren, Phys. Rev. E 78 (011502) (2008) 1.
[82] G.J. Brug, A.L.G. van den Eeden, M. Sluyters-Rehbach, J.H. Sluyters, J. Electroanal. Chem. 176 (1984) 275.
[83] T. Pajkossy, J. Electroanal. Chem. 300 (1991) 1.
[84] T. Pajkossy, J. Electroanal. Chem. 364 (1994) 111.
[85] Z. Kerner, T. Pajkossy, Electrochim. Acta 46 (2000) 207.
[86] H. Wang, L. Pilon, Electrochim. Acta (2011), doi:10.1016/j.electacta.2011.12.051, in press.
[87] G.C. Barker, J. Electroanal. Chem. 41 (1973) 201.
[88] K.T. Chu, M.Z. Bazant, Phys. Rev. E 74 (011501) (2006) 1.
[89] E.J.F. Dickinson, R.G. Compton, J. Electroanal. Chem. 655 (2011) 23.